Asian Journal of Chemistry; Vol. 37, No. 10 (2025), 2571-2577
ASIAN JOURNAL OF CHEMISTRY
https://doi.org/10.14233/ajchem.2025.34445

TiO_2-Anchored Graphene Nanocomposite as Robust Fluorometric Sensor for Ag^+ Ions and its Real Sample Analysis

A. PANDIYARAJAN[1], C.K. SUSHMA[2], DAVID JOHN DMONTE[1], S. VEERAMANI[2], B. VIDHYA[2,*] and R. NANDHAKUMAR[2,*]

[1]Department of Nanosciences and Technology, Karunya Institute of Technology and Sciences (Deemed-to-be University), Karunya Nagar, Coimbatore-641114, India
[2]Division of Physical Sciences, Karunya Institute of Technology and Sciences (Deemed-to-be University), Karunya Nagar, Coimbatore-641114, India

*Corresponding authors: E-mail: vidhya@karunya.edu; nandhakumar@karunya.edu

Received: 11 July 2025 *Accepted*: 23 September 2025 *Published online*: 30 September 2025 AJC-22142

A hybrid nanocomposite comprised of reduced graphene oxide and titanium dioxide (rGO-TiO_2) was synthesized from graphite following reduced graphene oxide synthesis, which utilized a modified Hummer's method and then subsequently reduced. The optical, morphological and structural properties of the hybrid composite were characterized with FTIR, UV-Vis, SEM, XRD and photoluminescence spectroscopy. The rGO-TiO_2 composite retains its in-solution affinity and selectivity for Ag^+ ions in an aqueous medium in spite of the presence of other metal ions. The sensing capabilities of this fluorometric sensor arise from the inhibition of photoinduced electron transfer mechanism (PET). The rGO-TiO_2 hybrid composite represents a low-cost, sensitive and effective sensing platform for the hazardous monitoring of metal ions under ambient conditions, particularly silver.

Keywords: Reduced graphene oxide, Silver ions, Chemosensor, Fluorescence, Water samples.

INTRODUCTION

Graphene [1], which is the 2D allotrope of carbon, consists of a monolayer of carbon atoms closely arranged in a hexagonal (honeycomb) lattice structure. Since its discovery, it has attracted tremendous scientific and technological curiosity due to its outstanding properties in many fields. These have excellent optical transparency [2], high thermal conductivity [3], exceptional mechanical stiffness and flexibility [4] and unprecedented electronic properties including high carrier mobility and electrical conductivity [5]. The oxidation of pristine graphene using oxygen-containing functional groups produce graphene oxide (GO) [6]. Graphene oxide (GO) can be chemically reduced to produce reduced graphene oxide (rGO) [7], which retains oxygen-containing functional groups and exhibits tunable physico-chemical properties. The members of graphene family (GO, rGO and carbon quantum dots (CQD)), have shown tremendous potential as sensors, especially in relation to their modifiable surface chemistry and unique optical behaviour [8]. Graphene oxide and rGO are considered to be effective materials for sensor development due to their high aqueous dispersibility, good biocompatibility, low toxicity and high chemical stability relative to traditional materials [9]. Moreover, in chemosensors, fluorescence-based sensing strategies have become popular due to their simplicity, sensitivity and affordability [10]. Graphene made from sp^2-hybridized carbon atoms has no band gap, making it non-fluorescent. By incorporating sp^3 hybridized oxygen-containing functional groups such as hydroxyl (-OH), carbonyl (C=O), epoxy (C-O-C) and carboxyl (–COOH), the material can exhibit enhanced fluorescence [11]. Specifically, the fluorescence characteristics may be controlled by altering the size of graphene oxide [12]. Silver ions (Ag^+) are used extensively in areas such as electronics [13], as antibacterial agents [14] and in pharmaceuticals [15].

Despite their widespread utility, silver ions and their nanoscale counterparts have drawn increasing attention due to growing concerns over their potential toxicity and detrimental effects on both environmental and human health [16]. Environmental exposure to Ag^+ is increasing as a result of improper disposal of industrial waste from manufacturing, accidental

spills and degradation of consumer products that contain silver nanoparticles [17]. Also, silver accumulation in the biological systems is associated with neurological and systemic health effects, indicating that sensitive and selective detection platforms for monitoring Ag^+ in soil and water ecosystems should be developed.

Several research groups have developed carbon-based fluorescent sensors to detect silver ions. Zhao *et al.* [18] developed a graphene quantum dots ratiometric fluorescent nano sensor for Ag^+ detection, whereas Li *et al.* [19] developed a carbon nanoparticle sensor for selective detection of Ag^+ ions. Based upon our initial findings and design consideration, in this work, we synthesized and functionalized a hybrid nanomaterial made of reduced graphene oxide (rGO) and titanium dioxide (TiO_2), referred to as rGO-TiO_2, as a fluorescent chemosensor. Its synthesis was designed to take advantage of the high surface area, great electron mobility and functional group diversity of rGO and bring in the great photostability. The intention was to develop this synergistic hybrid that would improve the photophysical behaviour of the sensor while having particular coordination sites for silver ion (Ag^+) recognition. The rGO-TiO_2 nanocomposite was prepared by a simple solution-based process entailing the hydrothermal growth of TiO_2 nanoparticles on the surface of chemically reduced graphene oxide sheets. Post-preparation functionalization was performed to allow the uniform dispersion of TiO_2 onto the rGO matrix and to develop reactive oxygen-containing groups able to selectively interact with Ag^+ ions. The produced nanohybrid displayed a stable fluorescence emission profile, which was utilized for chemosensing purposes [20].

EXPERIMENTAL

All chemicals and reagents employed were of analytical quality and used as such. The standard chemical sources were graphite powder, hydrogen peroxide, sodium nitrate, potassium permanganate, sodium borohydride, sulfuric acid and titanium dioxide. The X-ray diffraction (XRD) characterization was undertaken using Shimadzu X-600 X-ray diffractometer in the 2θ range of 10º to 70º with a scan rate of 10º min^{-1}. Surface morphology was observed and reported from a JEOL JSM-6390 scanning electron microscope (SEM). Functional groups were identified through Fourier transform infrared spectroscopy (FTIR) using Shimadzu Prestige-20 IR spectrometer in the wavenumber range of 4000-400 cm^{-1}. Using a JASCO V-650 UV-visible spectrophotometer and quartz cuvettes with a 1 cm path length, optical absorbance was measured. Photoluminescence (PL) were recorded with a JASCO FP-8200 Spectrofluorometer using 1 cm quartz cells.

Synthesis of graphene oxide: A modified Hummer's technique [21] was utilized to synthesize graphene oxide (GO). In a typical synthesis, 120 mL of conc. H_2SO_4 (95%) was mixed with 2.5 g of $NaNO_3$ and 5 g of powdered graphite in an ice bath under continuous stirring. After achieving a homogeneous mixture and maintaining the temperature below 20 ºC, 15 g of $KMnO_4$ was gradually added over 30 min. The mixture was stirred until it thickens and darkens, indicating the progression of oxidation. Then, 150 mL of distilled water was slowly added, causing the temperature to rise to approximately 98 ºC to further facilitate the oxidation. Once the mixture cooled to room temperature, 50 mL of 30% H_2O_2 was added to quench the reaction, resulting in a colour change. The suspension was stirred for an additional 3 h and then left undisturbed for 24 h to allow the sedimentation. The supernatant was removed by decantation and the remaining material was thoroughly washed with distilled water until a neutral pH was achieved. The resulting graphene oxide was then filtered and dried for subsequent use.

Synthesis of reduced graphene oxide: By employing sodium borohydride, the GO was reduced to reduced graphene oxide (rGO) [22,23]. A homogenous dispersion was prepared by ultrasonically dispersing approximately 0.3 g of GO into 100 mL of deionized water. A total of 0.4 g of $NaBH_4$ was added to this solution, heated to 100 ºC under reflux for 24 h, with moderate stirring. The product was collected by centrifugation, repeatedly washed with deionized water to remove any unreacted species, and the final precipitate was dried to obtain reduced graphene oxide (rGO).

Synthesis of rGO-TiO_2 nanocomposite: A solution-based reflux approach was used to prepare the rGO-TiO_2 nanocomposite. For thorough dispersion, each 500 mg of rGO and TiO_2 were separately dissolved in 100 mL of deionized water and sonicated for 30 min. Then, the two solutions were refluxed at 80 ºC for a whole day. Subsequently, the mixture was heated at 60 ºC in a hot-air oven until complete evaporation of water, yielding the solid rGO-TiO_2 nanocomposite.

Detection method: The detection of silver ions (Ag^+) was performed through fluorescence spectroscopic analysis using the synthesized rGO-TiO_2 nanocomposite as sensor material. Aqueous Ag^+ solutions of varying concentrations were freshly prepared and employed in a series of titration experiments to evaluate the sensor's performance. To each Ag^+ solution, a fixed volume of the rGO-TiO_2 nanocomposite dispersion was introduced, followed by gentle mixing and incubation at ambient room temperature to facilitate interaction between the analyte and the sensing matrix. Fluorescence emission spectra were recorded using a JASCO FP-8200 spectrofluorometer equipped with a quartz cuvette. The excitation and emission parameters were optimized to monitor changes in photoluminescence intensity corresponding to Ag^+ binding. The fluorescence response was found to increase with increasing concentrations of Ag^+, indicating a turn-on sensing mechanism likely arising from Ag^+-induced suppression of charge transfer quenching within the nanocomposite framework. To assess the selectivity of the sensor, comparative control experiments were carried out using a range of potentially interfering metal ions (*e.g.* Na^+, K^+, Ca^{2+}, Mg^{2+}, Cu^{2+}, Zn^{2+}, Fe^{3+}, Pb^{2+}). The photoluminescence intensity exhibited a significant and selective enhancement only in the presence of Ag^+ ions, demonstrating the high specificity of the rGO-TiO_2 nanocomposite toward silver ion detection.

Real sample analysis: The practical applicability of the rGO-TiO_2 nanocomposite based fluorescent probe was systematically evaluated through real-sample analysis to validate its accuracy, sensitivity and reliability in complex environmental matrices. To this end, the spike-and-recovery method was employed using water samples collected from various natural and domestic sources across different locations in Coimbatore, India. The selected samples included tap water, borewell water

and surface water, representing diverse physico-chemical environments. Known concentrations of Ag^+ ions were spiked into each sample to simulate contamination setups, followed by the addition of rGO-TiO_2 dispersion under optimized sensing conditions. After a brief incubation period at room temperature, the fluorescence emission spectra were recorded and the changes in photoluminescence intensity were used to quantify Ag^+ concentration. The recovery percentages were calculated by comparing the detected values with the known spiked concentrations.

RESULTS AND DISCUSSION

X-ray diffraction studies: The phase composition of the synthesized GO, rGO, TiO_2 and rGO-TiO_2 nanocomposite was characterized *via* X-ray diffraction as shown in Fig. 1. The peaks at 2θ = 10.10º and 43.10º, respectively indicate the oxidation of graphite and spacing between graphene sheets, consisting of oxygen-containing functional groups, in the graphene oxide XRD pattern. The peaks correspond to (001) and (100). The peaks disappeared after the reduction and two broad reflections indicating a partial reconstruction of the sp^2 carbon network of reduced graphene oxide (rGO) reappeared at 2θ = 25.69º and 43.57º. The X-ray diffraction (XRD) patterns of the synthesized TiO_2 sample present distinct peaks at 2θ of 25.21º, 38.40º, 47.92º, 54.90º and 62.56º indicative of the (101), (004), (200), (105) and (204) lattice planes, respectively. The close agreement between the diffraction peaks of the synthesized titania and the standard JCPDS card No. 21-1272 confirms the formation of pure anatase-phase titania. In case of the rGO-TiO_2 nanocomposite prepared by reflux methods, the XRD pattern exhibited only peaks at 2θ = 25.50º, 37.90º and 48.21º, indicating the presence of anatase TiO_2. The composite was not found to have any highly discernible diffraction peaks indicative of the presence of GO (characteristic peaks near roughly 10-12º) or rGO (characteristic peaks near 24-26º).

Morphological studies: The SEM image of rGO (Fig. 2a) exhibits thin, crumpled and wrinkled sheet-like structures similar to exfoliated graphene layers. These folded nanosheets are advantageous due to their high surface area and porosity, which provide an excellent framework for hosting nanoparticles. In Fig. 2b, pure TiO_2 particles appeared as tightly packed, quasi-spherical nanoparticles with a uniform average, promoting high crystallinity and size uniformity, as well as a degree of aggregation. The most pronounced difference occurs in the

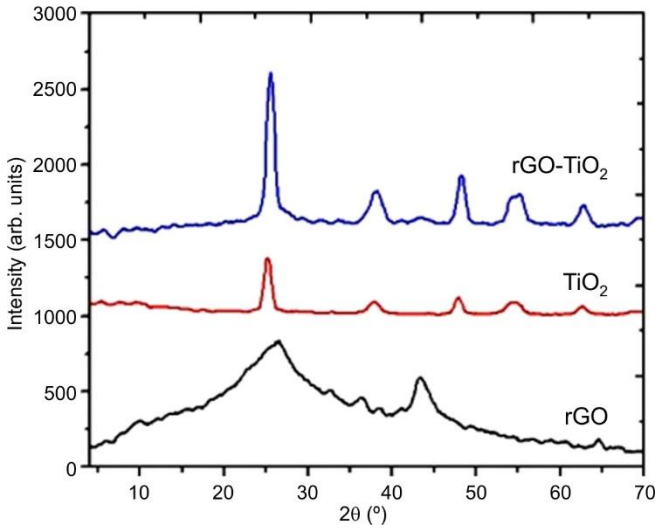

Fig. 1. XRD patterns of rGO, TiO_2 and rGO-TiO_2

rGO-TiO_2 composite (Fig. 2c), where nanoparticulate TiO_2 are uniformly anchored onto the rGO sheets without significant aggregation. The uniform distribution of TiO_2 across the rGO matrix implies that there are strong interfacial interactions realized through sonication and reflux. The rGO sheets serve as an effective dispersing scaffold, improving spatial separation of TiO_2 particles and improving contact at the surface level. The hybrid structure not only confirms the successful integration of rGO with TiO_2, but also suggests enhanced charge transfer characteristics, which are beneficial for sensing applications [24].

FTIR studies: The FTIR spectra of rGO, TiO_2 and rGO-TiO_2 nanocomposite (Fig. 3) was utilized to investigate the functional groups present in them. The rGO spectrum had peaks at 1675, 1555, 1227 and 1077 cm^{-1} is due to the C=O, C=C, C–OH and C–O vibrations, with the presence of oxygen containing functional groups and partial restore of graphitic domains [25]. The TiO_2 phase did not have any profile peaks as pure TiO_2 was a solid, though it had a broad band placed at 458.11 cm^{-1} which confirmed Ti–O bonds and O–Ti–O from the anatase phase [25]. The rGO–TiO_2 composite has characteristic bands at 458.11 cm^{-1} (Ti–O) and 514.05 cm^{-1} along with the 3531.81 and 1681.04 cm^{-1} (O–H stretching/bending) peaks and the two carbonyl/carboxyl peaks at 1519.97 and 1713.83 cm^{-1}. The presence of these features confirms that TiO_2 was successfully integrated onto the rGO plane and the

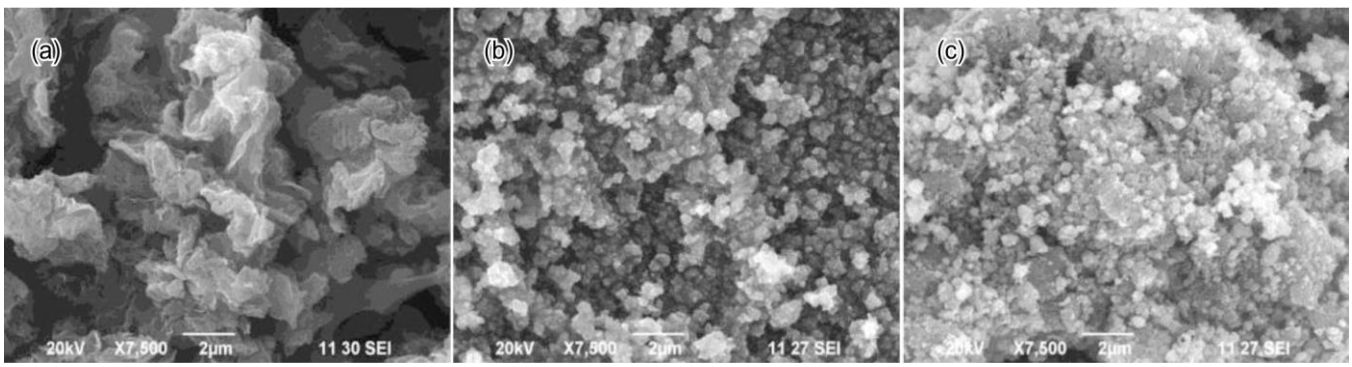

Fig. 2. SEM images of (a) rGO, (b) TiO_2 and (c) rGO-TiO_2

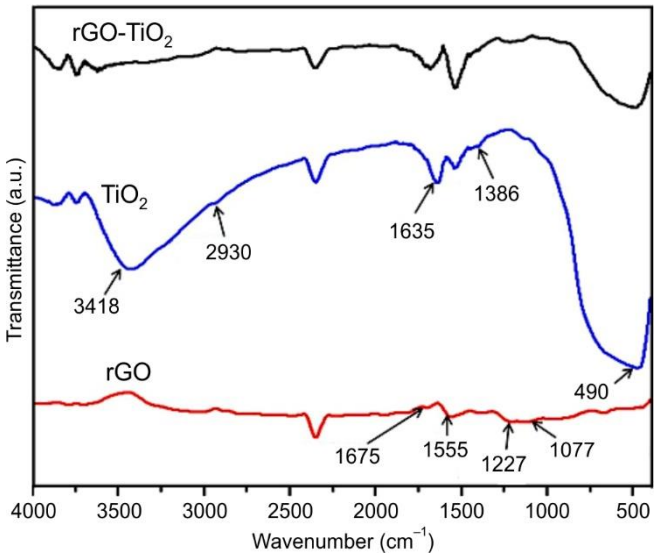

Fig. 3. FTIR spectra of rGO, TiO_2 and rGO-TiO_2

broader compatibility of the rGO-TiO_2 composite suggested there were strong inter-facial interactions that will enhance the sensing performance of the composite.

UV-visible absorption: The UV-vis spectra of reduced graphene oxide (rGO), TiO_2 and their rGO-TiO_2 composite (200-800 nm) reveal distinct features, for example, rGO shows a sharp π–π* peak at ~230 nm and an n–π* shoulder near ~300 nm, TiO_2 absorbs strongly around ~220 nm and the rGO-TiO_2 composite displays intensified bands at ~250 nm and ~320 nm (Fig. 4). These red-shifts and enhanced absorbance in the visible region indicate strong interfacial interactions likely Ti–O–C linkages that facilitate improved light absorption and charge separation, making the composite a promising candidate for photocatalytic applications [25,26].

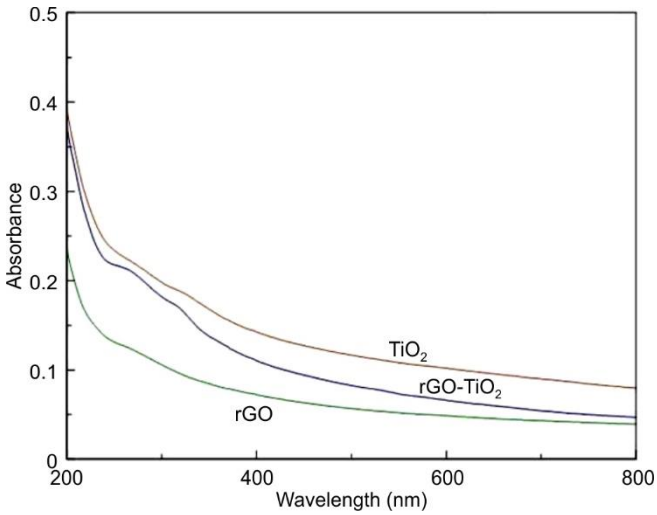

Fig. 4. UV spectra of TiO_2, rGO and GO-TiO_2

Photoluminescence studies: The photoluminescence spectra (Fig. 5) of the rGO, TiO_2 and rGO-TiO_2 composite (dispersed in water) shows two distinct emissions at ~420 nm and ~462 nm. The fluorescence intensity of the rGO-TiO_2 composite is substantially lower than the bare TiO_2, which indicates a reduced rate of electron–hole recombination. The

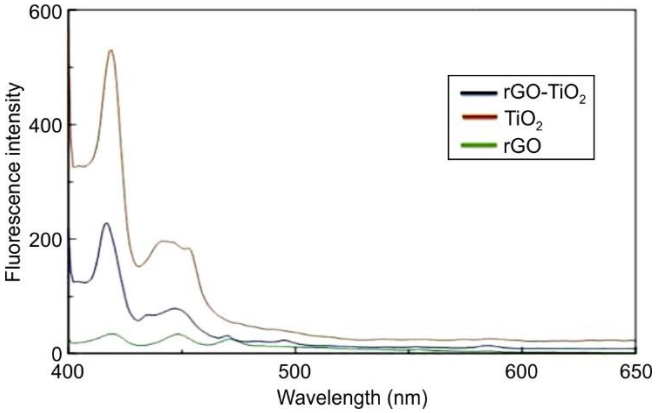

Fig. 5. PL spectra of TiO_2, rGO and GO-TiO_2

reduction observed in the recombination rate is due to efficient charge transfer to the graphene-based scaffold, which increases charge carrier lifetime and, in turn, photocatalytic ability [27].

Photoluminescence studies

Selectivity studies: Based on the preliminary UV-visible absorption studies (Fig. 6), the excitation wavelength for all subsequent fluorescence measurements was fixed at 395 nm, corresponding to the maximum absorption band of the rGO-TiO_2 nanocomposite probe. This wavelength ensured optimal excitation of the fluorophore component within the hybrid material, facilitating sensitive detection of Ag^+ ions. Importantly, the absorption spectra showed no evidence of red-shifted or broadened peaks typically associated with aggregation-induced effects, indicating that the nanocomposite remained well-dispersed in the working solution. The absence of aggregation formation ensures the consistency and reliability of the fluorescence response, eliminating potential artifacts that could compromise the sensitivity or specificity of the probe during sensing studies. The synthesized rGO-TiO_2 nanocomposite, as a chemosensor, is found to be non-fluorescent compound. However, when 100 equivalents of Ag^+ ions were successively added to the rGO-TiO_2 solution, an emission

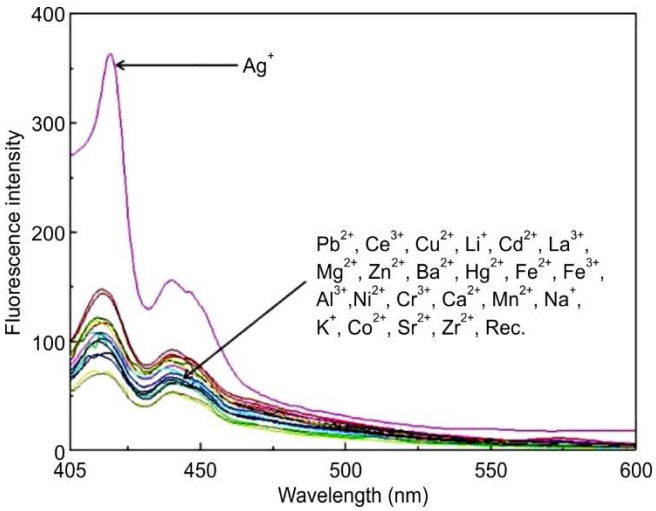

Fig. 6. Selectivity studies of rGO-TiO_2 (1) (5×10^{-6} M) in THF/H_2O (1:1 v/v, HEPES = 50 mM, pH = 7.4) in the existence of different metal ions (100 equiv. of each, excited at 395 nm)

peak at 420 was obtained with a substantial enhancement in the fluorescence intensity [28]. There were no observable differences in the fluorescence spectra for the selectivity of other metal ions such as Pb^{2+}, Ce^{3+}, Cd^{2+}, La^{3+}, Mg^{2+}, Zn^{2+}, Ba^{2+}, Hg^{2+}, Ag^{+}, Fe^{3+}, Fe^{2+}, Ni^{2+}, Cr^{3+}, Ca^{2+}, Mn^{2+}, Na^{+}, K^{+}, Cu^{2+} and Co^{2+} at the same concentration, therefore, the rGO-TIO_2 based off-on probe is primarily sensing Ag^{+} in THF-H_2O (1:1 v/v) and pH = 7.4 (HEPES = 50 mM) solution.

Interference studies: Competitive metal ion analysis was performed to evaluate the selectivity of the rGO-TiO_2 fluorescence sensor toward Ag^{+} ions. In this study, solutions containing probe **1** (rGO-TiO_2) and Ag^{+} (100 equiv.) were mixed with various potentially interfering metal ions, including Pb^{2+}, Ce^{3+}, Cd^{2+}, La^{3+}, Mg^{2+}, Hg^{2+}, Zn^{2+}, Ba^{2+}, Fe^{3+}, Cr^{3+}, Fe^{2+}, Ni^{2+}, Ca^{2+}, Mn^{2+}, Na^{+}, K^{+}, Co^{2+} and Cu^{2+} (Fig. 7). The red bars in the figure represent the fluorescence emission responses of chemosensor **1** (rGO–TiO_2) to individual metal ions (1–100 equiv.), while the blue bars indicate the fluorescence changes when these metal ions (100 equiv.) were added to the preformed rGO–TiO_2–Ag^{+} (100 equiv.) complexes. The results clearly demonstrate that even in the presence of a wide range of competitive metal ions, rGO–TiO_2 exhibits strong fluorescence selectivity toward Ag^{+} ions, showing the minimal interference from other tested species. This highlights its potential as a highly selective and robust fluorescence sensor for the detection of silver ion [29].

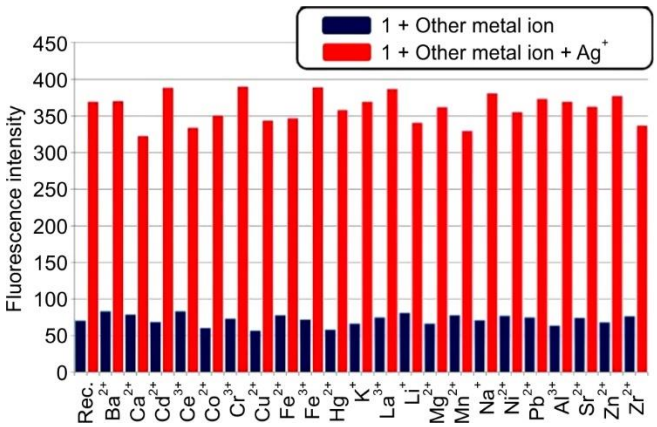

Fig. 7. Metal ion competitive analysis of rGO-TiO_2 (1) (5×10^{-6} M) in THF/H_2O (1:1 v/v, HEPES = 50 mM, pH = 7.4) in the existence of different metal ions (100 equiv. of each, excited at 395 nm)

Fluorescence titration: Fluorescence titrations were also conducted to investigate the interaction between rGO-TiO_2 and Ag^{+} ions, with the resulting emission spectra presented in Fig. 8. Upon gradual addition of Ag^{+} ions (0–100 equiv.) to the rGO–TiO_2 solution, a progressive enhancement in fluorescence intensity was observed. This enhancement indicates a strong and concentration-dependent interaction between Ag^{+} and the rGO-TiO_2 sensor system. Notably, the fluorescence response reached near-saturation at approximately 50 equiv. of Ag^{+}, suggesting that the available active sites on the rGO-TiO_2 surface become effectively occupied at this concentration level. Beyond this point, additional Ag^{+} ions induced the minimal changes in fluorescence, indicating a saturation binding behaviour consistent with a high-affinity and selective interaction mechanism [30]. The detection limit (LOD) of

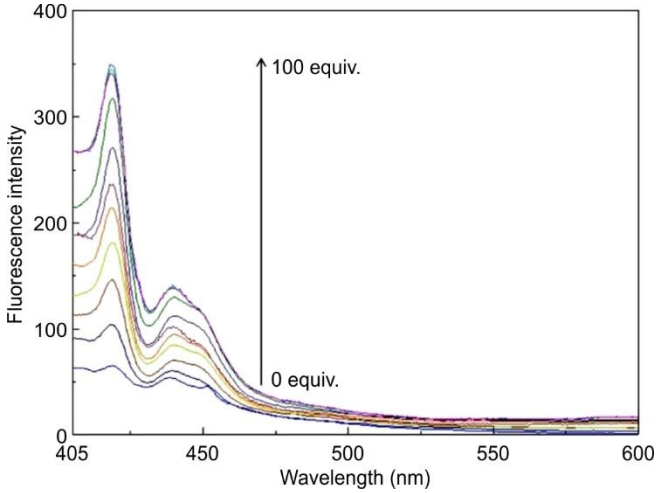

Fig. 8. Fluorescence spectral changes of probe rGO-TiO_2 (1) (5×10^{-6} M) with various concentration of Ag^{+} ions (0 to 100 equivalents) in THF/H_2O (1:1 v/v, HEPES = 50 mM, pH = 7.4) solution

chemosensor was determined as 0.35×10^{-5} M and was calculated using 3δ/S, where δ denotes standard deviation of the blank signal and S denotes slope of the linear calibration plot.

Time response: The time-dependent fluorescence response of the rGO-TiO_2 based sensor toward Ag^{+} ions was evaluated and the results are illustrated in Fig. 9. This experiment aimed to assess the kinetics of complex formation between the receptor and Ag^{+} ions under ambient conditions. Upon addition of 100 equiv. of Ag^{+}, a significant and rapid increase in fluorescence intensity was observed, reaching a maximum steady-state value within approximately 4 min. This rapid response suggests that the complexation process between rGO-TiO_2 and Ag^{+} is both efficient and fast, likely governed by favourable surface interactions and diffusion-controlled kinetics. After 4 min, no further appreciable changes in fluorescence intensity were detected indicating that the complexation had reached completion and that the system had achieved fluorescence saturation. This behaviour confirms the rapid response capability of the rGO-TiO_2 sensor, making it suitable for real-time or on-site detection of Ag^{+} ions [31].

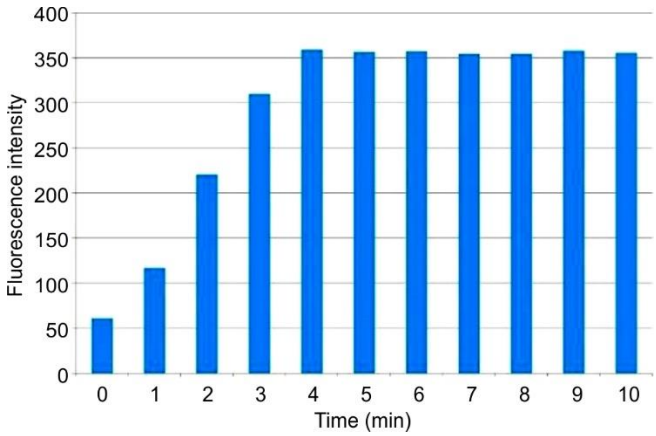

Fig. 9. Effect of time effect of the receptor rGO-TiO_2 1 (5×10^{-6} M) solution in THF/H_2O (1:1 v/v, HEPES = 50 mM, pH = 7.4) solution

Effect of pH: The pH-dependent sensing performance of the probe rGO-TiO_2 for Ag^{+} detection was systematically

investigated under two distinct conditions *viz*. (i) in absence of Ag^+ and (ii) in the presence of Ag^+ ions. The pH of the medium was precisely adjusted using dilute solutions of HCl and NaOH to span a wide range of values. As illustrated in Fig. 10, the fluorescence response of rGO-TiO_2 composite in the presence of Ag^+ remained in the "turn-on" state across a broad pH window ranging from 4.0 to 10.5. In contrast, the system exhibited a distinct "turn-off" state under more acidic (pH < 4.0) and highly alkaline (pH > 10.5) conditions, indicating protonation/deprotonation effects or possible structural destabilization of the sensing interface under extreme pH environments. This observation confirms that the rGO-TiO_2 sensor maintains stable and effective Ag^+ detection across a wide range of physiologically and environmentally relevant pH conditions. The robustness and responsiveness of the sensor in such a broad pH window significantly enhance its practical applicability for real-world sensing applications, including environmental monitoring, biological fluid analysis and industrial wastewater assessment [32].

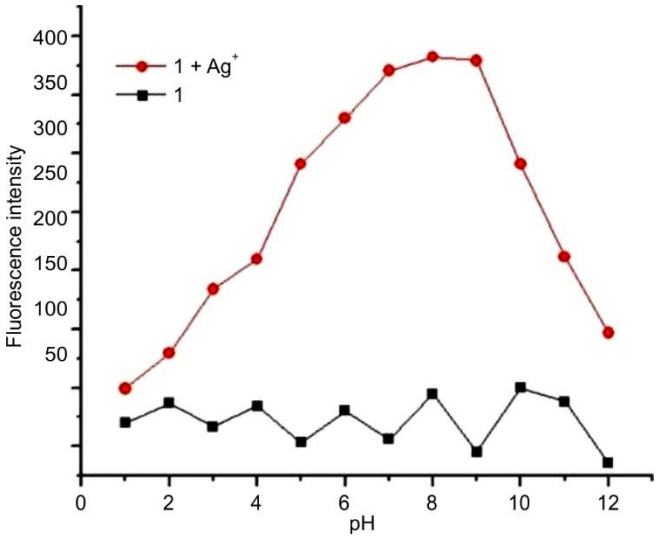

Fig. 10. Effect of pH of the probe rGO-TiO_2 (**1**) in presence and absence of Ag^+ ions

Applications

Real water sample analysis: Following the successful establishment of the binding affinity between the rGO-TiO_2 nanocomposite probe and Ag^+ ions through fluorescence studies, we extended our investigation to real sample analysis to evaluate the practical utility and field applicability of the developed sensor. For this purpose, a variety of environmental water samples, known to either contain or be vulnerable to silver ion contamination, were carefully selected from different locations across Coimbatore city, India. These included tap water, borewell water and surface water samples from both urban and peri-urban regions. To assess the sensor's accuracy and reliability in complex matrices, recovery experiments were performed using the standard spike-and-recovery approach. Known concentrations of Ag^+ ions were spiked into each sample and the rGO-TiO_2 probe was used to quantify the recovery of Ag^+ under ambient conditions. The primary objective of these studies was to determine the ability of the rGO-TiO_2 sensor to detect Ag^+ ions with high sensitivity and selectivity in real-world samples. The detection limit and recovery percentages obtained are summarized in Table-1.

The sensor demonstrated excellent recovery efficiencies, with the highest observed value reaching 98%, underscoring its capability for accurate detection in environmental matrices. Furthermore, the detection limit calculated from the fluorescence titration studies was found to be in the sub-micromolar range, making it suitable for trace-level monitoring of Ag^+ contamination. To validate the performance of the fluorescence-based detection method, parallel quantitative analyses were conducted using ICP-MS. The same spiked samples were subjected to ICP-MS measurements, which enabled precise quantification of Ag^+ ions based on their mass-to-charge (*m*/*z*) ratios. A comparative analysis between the fluorescence sensing data and ICP-MS results revealed strong correlation and consistency, thereby confirming the accuracy and reliability of the developed rGO-TiO_2 probe. Collectively, these findings demonstrate that the rGO-TiO_2 nanocomposite is not only highly sensitive and selective toward Ag^+ ions in controlled laboratory conditions but also exhibits robust performance in complex, real-world water samples. Its compatibility with field-relevant matrices and agreement with gold-standard techniques like ICP-MS strongly support its potential as a practical and cost-effective tool for environmental monitoring and contamination assessment.

Conclusion

In this work, rGO-TiO_2 nanocomposite exhibited remarkable effectiveness as a fluorescence-based chemosensor for the analysis of Ag^+ in aqueous solutions. The tripartite response from the composite with Ag^+ underwent an "off-to-on" shift using visible excitation. Upon excitation a dark material develops a strong emission of light at ~420 nm, only after the addition of Ag^+. This type of response can be attributed to the inhibition of photoinduced electron transfer (PET) mechanism where the binding of Ag^+ prevents the PET from rGO to TiO_2 causing emission of fluorescence. Probe rGO-TiO_2 efficiently detected Ag^+ in water samples.

TABLE-1
DETECTION OF Ag^+ ION IN VARIOUS WATER SAMPLES USING PROBE rGO–TiO_2 (**1**)

Sample	Fluorescence analysis					ICP-MS		
	Spiked	Found	Recovery (%)	LOD (μM)	RSD	Found	Recovery (%)	RSD
Cavery	0.02	0.018 ± 0.002	92	1.82	1.09	0.019 ± 0.001	97	1.04
Borewell	0.02	0.019 ± 0.001	95	2.33	1.20	0.019 ± 0.001	95	1.20
Siruvani	0.02	0.019 ± 0.001	96	1.01	1.57	0.019 ± 0.001	98	1.56
Ukkadam lake	0.02	0.019 ± 0.001	97	1.11	1.55	0.018 ± 0.002	94	1.60

ACKNOWLEDGEMENTS

Two of the authors, CKS and SV, are thankful to Karunya Institute of Technology and Sciences (Deemed to be University) for providing the financial support through research associateship fellowship.

CONFLICT OF INTEREST

The authors declare that there is no conflict of interests regarding the publication of this article.

REFERENCES

1. K.S. Novoselov, A. Mishchenko, A. Carvalho and A.H. Castro Neto, *Science*, **353**, aac9439 (2016); https://doi.org/10.1126/science.aac9439
2. Z. Sun, A. Martinez and F. Wang, *Nat. Photonics*, **10**, 227 (2016); https://doi.org/10.1038/nphoton.2016.15
3. Z. Yan, D.L. Nika and A.A. Balandin, *IET Circuits Devices Syst.*, **9**, 4 (2015); https://doi.org/10.1049/iet-cds.2014.0093
4. J. Chen, H. Bi, S. Sun, Y. Tang, W. Zhao, T. Lin, D. Wan, F. Huang, X. Zhou, X. Xie and M. Jiang, *ACS Appl. Mater. Interfaces*, **5**, 1408 (2013); https://doi.org/10.1021/am302825w
5. Y. Liang, X. Liang, Z. Zhang, W. Li, X. Huo and L. Peng, *Nanoscale*, **7**, 10954 (2015); https://doi.org/10.1039/C5NR02292D
6. M.F.R. Hanifah, J. Jaafar, M. Aziz, A.F. Ismail, M.A. Rahman and M.H.D. Othman, *J. Teknologi*, **74**, 189 (2015); https://doi.org/10.11113/jt.v74.3555.
7. N. Cao and Y. Zhang, *J. Nanomaterials*, **2015**, 168125 (2015); https://doi.org/10.1155/2015/168125
8. S. Zhu, J. Zhang, X. Liu, B. Li, X. Wang, S. Tang, Q. Meng, Y. Li, C. Shi, R. Hu and B. Yang, *RSC Adv.*, **2**, 2717 (2012); https://doi.org/10.1039/c2ra20182h
9. S. Gurunathan and J.-H. Kim, *Int. J. Nanomedicine*, **11**, 1927 (2016); https://doi.org/10.2147/IJN.S105264
10. D. Wu, A.C. Sedgwick, T. Gunnlaugsson, E.U. Akkaya, J. Yoon and T.D. James, *Chem. Soc. Rev.*, **46**, 7105 (2017); https://doi.org/10.1039/C7CS00240H
11. J. Shang, L. Ma, J. Li, W. Ai, T. Yu and G.G. Gurzadyan, *Sci. Rep.*, **2**, 792 (2012); https://doi.org/10.1038/srep00792
12. S. Zhu, S. Tang, J. Zhang and B. Yang, *Chem. Commun.*, **48**, 4527 (2012); https://doi.org/10.1039/c2cc31201h
13. I.J. Fernandes, A.F. Aroche, A. Schuck, P. Lamberty, C.R. Peter, W. Hasenkamp and T.L.A.C. Rocha, *Sci. Rep.*, **10**, 8878 (2020); https://doi.org/10.1038/s41598-020-65698-3
14. S. Medici, M. Peana, G. Crisponi, V.M. Nwurchi, J.I. Lachowicz, M. Remelli and M.A. Zoroddu, *Coord. Chem. Rev.*, **327–328**, 349 (2016); https://doi.org/10.1016/j.ccr.2016.05.015
15. P. Mathur, S. Jha, S. Ramteke and N.K. Jain, *Artif. Cells Nanomed. Biotechnol.*, **46(sup1)**, 115 (2018); https://doi.org/10.1080/21691401.2017.1414825
16. H.T. Ratte, *Environ. Toxicol. Chem.*, **18**, 89 (1999); https://doi.org/10.1002/etc.5620180112
17. E. McGillicuddy, I. Murray, S. Kavanagh, L. Morrison, A. Fogarty, M. Cormican, P. Dockery, M. Prendergast, N. Rowan and D. Morris, *Sci. Total Environ.*, **575**, 231 (2017); https://doi.org/10.1016/j.scitotenv.2016.10.041
18. X.-E. Zhao, C. Lei, Y. Gao, H. Gao, S. Zhu, X. Yang, J. You and H. Wang, *Sens. Actuators B Chem.*, **253**, 239 (2017); https://doi.org/10.1016/j.snb.2017.06.086
19. H. Li, J. Zhai, and X. Sun, *Langmuir*, **27**, 4305 (2011); https://doi.org/10.1021/la200052t
20. D.J. Dmonte, A. Pandiyarajan, N. Bhuvanesh, S. Suresh and R. Nandhakumar, *Mater. Lett.*, **227**, 154 (2018); https://doi.org/10.1016/j.matlet.2018.05.051
21. S.N. Alam, N. Sharma and L. Kumar, *Graphene*, **6**, 1 (2017); https://doi.org/10.4236/graphene.2017.61001
22. H.-J. Shin, K.K. Kim, A. Benayad, S.-M. Yoon, H.K. Park, I.-S. Jung, M.H. Jin, H.-K. Jeong, J.M. Kim, J.-Y. Choi and Y.H. Lee, *Adv. Funct. Mater.*, **19**, 1987 (2009); https://doi.org/10.1002/adfm.200900167
23. J. Chen, B. Yao, C. Li and G. Shi, *Carbon*, **64**, 225 (2013); https://doi.org/10.1016/j.carbon.2013.07.055
24. H. Zhang, X. Lv, Y. Li, Y. Wang and J. Li, *ACS Nano*, **4**, 380 (2010); https://doi.org/10.1021/nn901221k
25. K. Porkodi and S.D. Arokiamary, *Mater. Charact.*, **58**, 495 (2007); https://doi.org/10.1016/j.matchar.2006.04.019
26. Q. Lai, S. Zhu, X. Luo, M. Zou and S. Huang, *AIP Adv.*, **2**, 032146 (2012); https://doi.org/10.1063/1.4747817
27. C. Basheer, *J. Chem.*, **2012**, 456586 (2012); https://doi.org/10.1155/2013/456586
28. K. Velmurugan, S. Suresh, S. Santhoshkumar, M. Saranya and R. Nandhakumar, *Luminescence*, **31**, 722 (2016); https://doi.org/10.1002/bio.3016
29. B.N. Revanna, V. Kamat, A. Swamynayaka, K.K. Harish, K. Venkatesha, M. Madegowda, B. Poojary, S.S. Majani and S.P. Kollur, *J. Fluoresc.*, **35**, 1781 (2025); https://doi.org/10.1007/s10895-024-03646-4
30. J. Prabhu, K. Velmurugan, Q. Zhang, S. Radhakrishnan, L. Tang and R. Nandhakumar, *J. Photochem. Photobiol. Chem.*, **337**, 6 (2017); https://doi.org/10.1016/j.jphotochem.2017.01.006
31. J. Prabhu, K. Velmurugan and R. Nandhakumar, *J. Anal. Chem.*, **70**, 943 (2015); https://doi.org/10.1134/S1061934815080134
32. K. Velmurugan and R. Nandhakumar, *J. Lumin.*, **162**, 8 (2015); https://doi.org/10.1016/j.jlumin.2015.01.039